A non contact measurement technique for the density and the thermal expansion coefficient of solid and liquid materials

Sang K. Chung, David B. Thiessen[a] and Won-Kyu Rhim

Jet Propulsion Laboratory, California Institute of Technology, 4800 Oak Grove Drive, Pasadena, California 91109

a) Present address: Washington State University, Physics Department, Pullman, WA 99164.

ABSTRACT

A non contact measurement technique for the density and the thermal expansion coefficient of undercooked and superheated materials as well as the solid materials is presented. The experiments were performed using the high-temperature high-vacuum electrostatic levitator (HTHVESL) at JPL in which 2-3 mm diameter samples can be levitated, melted using a focused xenon lamp, and radiatively cooled in vacuum. Due to the axisymmetric nature of the molten samples when levitated in the HTHVESL system, a rather simple digital image analysis can be employed to accurately measure the volumetric change as a function of temperature. Density measurements were made on Ni in the temperature range 1045 to 1565 C in order to test the accuracy of the technique. Densities were computed from a sequence of images taken during a containerless processing run in which the Ni sample cools from 110 degrees above the melting point into the undercooked liquid state followed by recalescence and further cooling. A sharp discontinuity in the density was observed at the time of recalescence.

INTRODUCTION

Density is one of the most fundamental properties of a material. It is intrinsically related to other thermophysical properties. The density and the thermal expansion coefficient are important parameters in understanding material behavior in the liquid or solid state. The modern electronic materials industries, for example, are trying to enhance their understanding of a variety of semiconductor melts for the production of higher quality crystals. The density and thermal expansion coefficient as a function of temperature are basic parameters needed to numerically model processing situations.'

While accurate density measurement is relatively simple for solid materials at room temperature, it is nontrivial for high temperature molten materials. A number of techniques have traditionally been used to measure the density of high temperature melts. Among these techniques are the archimedian,[2,6] maximum bubble pressure,[2,7] sessile drop,[2] pycnometric[2] and dilatometric[2] methods. Beginning in the 1960s, containerless methods utilizing electromagnetic levitators (EML) began to emerge. The EML method involved photographing an axisymmetric sample from a direction perpendicular to the symmetry axis. The sample volume was calculated by integrating the cross sectional area with respect to the vertical coordinate (symmetry axis).[3,4] The primary advantage of containerless methods for measuring the density of high temperature melts is that it reduces heterogeneous nucleation which is primarily caused by contact with container walls. This extends the temperature domain of the density measurement to deeply undercooked regions. Another advantage of the containerless method is that sample contamination by the crucible material is avoided. Such contamination may affect the measurements for certain materials. Containerless methods used until the present have relied exclusively on EML. With the recent development of HTHVESL[5] a new approach to containerless density measurement became possible. Some of the drawbacks with the EML systems used in measuring the density of the sample are (i) The stirring effects of the liquid sample caused by the interaction between the eddy currents and the applied rf fields tend to distort the sample shape quite severely so that the sample volume calculation becomes very complicated and inaccurate. Due to this effect one author reported that only 2°/0 of the collected images turned out to be useful for the volume measurement.[3] (ii) The test sample is limited to electrical conductors, unless the sample is treated by deliberately adding undesirable electrically conductive agents; therefore, almost all the family of nonconductors and semiconductors are excluded from this type of density measurement technique. (iii) The very structure of the EML system, due to its closely

wound coils around the sample, make imaging of the sample very difficult. (iv) Heating and levitation are strongly coupled in the EML system, making it very difficult to measure the density of materials with low melting point. With the HTHVESL system all of the above difficulties can be resolved. Due to the active position control used in the HTHVESL system, the levitated sample is extremely stable (1 O μm), and the geometry of the force field around the levitation electrodes induce the sample shape to stay axisymmetric when it is in the liquid form. Due to the axisymmetric nature of the molten sample, only a single image is required to extract the volume information. This makes the volume calculation extremely simple and reliable. The use of modern digital image processing techniques combined with high resolution CCD video cameras allows the volume calculations to be done automatically.

In this article we describe for the first time, a containerless density measurement technique utilizing the HTHVESL system and digital image analysis. The basic technique involves recording a digital image of the drop from a direction perpendicular to the symmetry axis. The digital image is analyzed to locate the edge of the drop, producing a set of four hundred edge coordinates. The edge coordinates are fit with the axisymmetric spherical harmonic functions through sixth order using a least squares method. The image analysis techniques used here are similar to those which have been used for pendant drop surface tension measurements Once the coefficients of the spherical harmonic functions have been determined by fitting the edge coordinates, it is a trivial matter to integrate this function to obtain the drop volume. The density can then be calculated provided the mass of the sample is known. The thermal expansion coefficient can be calculated if the volume is measured over a range of temperatures. The underlying definitions are:

$$\rho = m / V, \tag{1}$$

$$\beta = \frac{1}{V}\left(\frac{\partial V}{\partial T}\right). \tag{2}$$

where ρ is the density, m is the mass, V is the volume, β is the thermal expansion coefficient and T is the sample temperature. For a sample that is radiatively cooled in vacuum:

$$dQ / dt = -A\,\sigma\,\varepsilon_T\,(T^4 - T_b^4), \tag{3}$$

where dQ/dt is the cooling rate, A is the sample surface area, σ is the Stefan-Boltzmann constant, ε_T is the total hemispherical emissivity, T is the sample temperature and Tb is the background temperature.

We have demonstrated the validity of this new containerless density measurement technique utilizing HTHVESL, by performing experiments with Ni. The results obtained for Ni are compared with the results from previous EML studies and other works.

EXPERIMENTAL

HARDWARE

The experiments were performed using the high-temperature high-vacuum electrostatic levitator (HTHVESL) at the Jet Propulsion Laboratory.[5] Figure 1 shows a schematic diagram of the HTHVESL system plus some additional imaging devices used for measurement of the density of the levitated molten materials. The HTHVESL consists primarily of a set of parallel electrodes in which samples of 2-3 mm diameter can be levitated while being actively controlled for position stability. The electrodes are placed inside the stainless steel vacuum chamber which is typically evacuated to 10^{-7} torr. The sample is heated using a focused 1 kW xenon arc lamp (PS1OOOSW-1 : ILC Technology) which is capable of raising the sample temperature to about 2300 K. Since the electrostatic levitation is not coupled to the sample heating, the sample can be allowed to cool to room temperature by extinguishing the arc lamp. The cooling phase therefore, is strictly radiative.[5] To measure the temperature of the levitated sample, a non-contact single color pyrometer (custom made) operating at 750 nm (filter width: ~10 nm FWHM) and set to 60 Hz bandwidth was used. The pyrometer incorporates a photomultiplier tube along with a log ratio amplifier for high sensitivity at all temperature ranges. The wavelength chosen for the pyrometer overlapped with the spectrum of the xenon arc lamp; therefore, the experiment had to be carried out during the cooling period while the arc lamp is completely covered or shut off. A single-reflex view finder attached to the pyrometer was equipped with a visual target area which is directed to the point of interest on the surface of the sample. The target spot on the sample viewed by the pyrometer was about 1 mm in diameter. The radiance from the sample is converted to temperature using Wien's formula. The constants that enter the equation are obtained by calibration with a black body source at several different temperatures. The sample temperature is then calibrated at the melting point of the sample by adjusting the emissivity of the pyrometer.

The accuracy of the density measurements is critically dependent on the imaging system. The image capture and analysis utilized a high resolution (570 x 485) black and white CCD video camera (Hitachi Denshi, Ltd : Model KP-M1) and a 8 bit gray scale video frame grabber board (Data Translation : QuickCapture) which plugged into the Nu-Bus slot of the Macintosh computer (Apple : Quadra 950). It has the on-board video memory to store one *640 x 480* element image. In order to magnify the image of a small levitated drop at a minimum working distance of 20 cm, the CCD camera was attached to a long distance microscope (Infinity : Model K2) via C-mount. This microscope allows the image of the drop to fill the full view of the CCD chip for accurate analysis. An intense, collimated fiber optical light source (Fiberoptic Specialties, Inc. :250 Watt) was used to back light the levitated sample in order to obtain a high-contrast image. In order to prevent the CCD camera from being saturated by the background light, the shutter speed of the camera was maintained at 1/10000 of a second to reduce the integration of the light falling onto the CCD sensor. This procedure in addition, helped to eliminate the blurring of the image caused by the residual vibrations from the floor and the position control of the sample. To block the scattered light from the position feedback laser that reflected off the surface of the sample, a HeNe line blocking filter is inserted in the optical path between the sample and the microscope. A separate Macintosh II computer equipped with a video overlay card (Computer Friends : TV Producer) is used to superimpose the time and temperature information on the CCD image. A video cassette recorder (VCR) is used to record the video image for post processing. A video time base corrector (SONY : MPU-F100) is used to stabilize the paused frame transfer from VCR to computer.

SOFTWARE

The architecture of the density measurement software is shown in Fig. 2 in a flow chart format. Software tasks are divided into four groups: IMAGE CAPTURE, IMAGE ANALYSIS, IMAGE CALIBRATION and IMAGE OVERLAY. Among these groups the first three are integrated into a single unit so that the user can go back and forth easily from one to another. The IMAGE OVERLAY program is designed to run separately during the entire experiment.

The IMAGE CAPTURE software is a custom made device driver, specifically used with the QuickCapture frame grabber board that sits inside the Macintosh Quadra 950 computer. Its function is to grab a video frame and store it as a custom formatted digital image file on the hard disk. The IMAGE CAPTURE software can be operated in two different modes: the live mode and the post-processing mode. Live mode enables

the user to capture sequential images of the sample during the passive cooling phase directly from the CCD camera to the computer hard disk at a fixed frame rate until a pre-assigned, low-temperature limit is reached. Since each image requires 512K bytes of disk space, experiments use up hard disk space very quickly when operated in live mode. The hardware used in this work limits the speed of live image acquisition to 2.5 frames/second. The post-processing mode enables the user to capture sequential images from the VCR after the whole experiment has been recorded on a video cassette. The advantage of the latter method is that a higher frame rate can be achieved (30 frames/second) which makes possible the analysis of samples with higher cooling rates. Hard-disk space is saved by acquiring and analyzing a single image at a time, deleting the particular image file once the volume is calculated, and then proceeding to capture the next image recorded on the video tape. The disadvantage of post-processing is that the images recorded on video tape suffer some 10ss of quality.

The post-processing method requires that time and temperature data be recorded to the video cassette in synchronization with the images. The IMAGE OVERLAY software superimposes time, temperature, and other information on the CCD image in a format similar to Fig. 3. The time and the temperature readouts are updated faster than 30 frames/second so that each frame has the proper information.

The IMAGE ANALYSIS software is used to compute sample volumes from the digital images. The analysis program is divided into two parts: edge detection and volume analysis. The edge detection algorithm finds the edge of the sample image against the background by using the intensity gradient. The volume analysis algorithm fits the detected edge points with a theoretical curve and integrates the theoretical curve to find the volume. The detailed method will be discussed in the next section.

The IMAGE CALIBRATION software is used to analyze a digital image of a levitated precision calibration sphere of known diameter in order to determine horizontal and vertical magnification factors for the sample images. This software utilizes some of the same routines as the IMAGE ANALYSIS software described above. The edge detection algorithm is used to find the edge of the calibration sphere and the data is fit with the spherical harmonic functions. The horizontal and vertical diameters in pixels are determined from the fit profile. The horizontal and vertical magnification factors are then obtained as the ratio of the known diameter to the diameters in pixels. Finally, the obtained magnification factors are recorded in a calibration file which is referenced whenever the volume analysis is performed.

MEASUREMENT TECHNIQUE

The digital images of levitated drops are analyzed by the IMAGE ANALYSIS software to compute the drop volume. The first step in this process is to locate the edge of the drop. A set of 400 equally spaced radial vectors are created centered on the approximate drop center, (x_0, y_0),

$$\left.\begin{aligned} x_{ij} &= r_i \sin\theta_j + x_0 \\ y_{ij} &= r_i \cos\theta_j + y_0 \\ \theta_j &= 2\pi j / 400 \end{aligned}\right\} \quad j=1,\ldots,400$$
$$r_i = i\,\delta r, \qquad \delta r = 1 \tag{4}$$

where x and y are the horizontal and vertical coordinates respectively. The intensity at spacings of one pixel along each vector is determined using bilinear interpolation of the adjacent pixel intensities. The drop edge is detected by searching for the maximum intensity gradient along each vector to yield a set of 400 edge points, (x_j, y_j). The average of the x and y coordinates of the edge points is taken as a new estimate of the drop center. New radial vectors are set up centered on this new estimate of x_0 and y_0 and edge detection is repeated once more.

The edge points are fit with the spherical harmonic functions through sixth order to provide a smooth profile for volume integration.

$$R(\theta) = \sum_{n=0}^{6} c_n P_n^0(\cos\theta) \tag{5}$$

where $P_n^0(\cos\theta)$ are the nth order Legendre polynomials evaluated at cos 8, and c_n are the unknown coefficients which must be determined by a fitting procedure. The experimental edge coordinates are converted to polar coordinates,

$$\begin{aligned} R_j &= \left[(x_j - X_0)^2 L_x^2 + (y_j - Y_0)^2 L_y^2\right]^{1/2} \\ \theta_j &= \sin^{-1}\left[\frac{(x_{ji} - X_0)L_x}{R_j}\right] \end{aligned} \tag{6}$$

where L_x and L_y are the horizontal and vertical magnification factors (cm/pixel) determined from the calibration procedure. The following objective function is minimized to determine the coefficients of the Legendre polynomials,

$$F(X_0, Y_0, c_0, \ldots, c_6) = \sum_{j=1}^{400} \left[\frac{R_j - R(\theta_j)}{\sigma_j} \right]^2, \tag{7}$$

where X. and Y. are the pixel coordinates of the origin of the polar coordinate system, and σ_j is the measurement error of the jth data point. The values of X_0 and Y_0 are initialized to the average x and y coordinates of the experimental edge points. The objective function F is minimized with respect to X. and the coefficients c_0 through c_6. The fitting function $R(\theta)$ given by Eq. (5) is linear in the coefficients thus allowing for a linear least squares method to determine the optimal values of the coefficients for a given value of X_0. A one-dimensional minimization of F with respect to X_0 is performed using a parabolic interpolation algorithm. Each time X. is changed, the polar coordinates of the experimental edge points are recomputed according to Eq. (6) and F *is* minimized with respect to the Legendre polynomial coefficients by linear least squares. The parameter Y_0 does not need to be optimized since the fitting function can accomadate a vertical shift in the coordinate system.

Following optimization of the coefficients of the Legendre polynomials, the volume is computed by integrating the optimal profile as follows:

$$V = \frac{2\pi}{3} \int_0^{\pi} R(\theta)^3 \sin\theta \, d\theta. \tag{8}$$

A rough estimate of the error in the volume calculation arising from random errors in the position of the edge points can be obtained by (considering the uncertainty in $R(\theta)$. For a spherical sample, an uncertainty in f? of δR leads to an uncertainty in volume of $4\pi R^2 \delta R$. The relative error in the volume is then

$$\frac{\delta V}{\mathbf{V}} \frac{4}{=} \frac{\pi R^2 \delta R}{4\pi R^3 / 3} = \frac{3\delta R}{R} \tag{9}$$

A typical image of a molten Ni sample gives R = 160 pixels. If δR is taken to be one pixel, then the percent uncertainty in the volume is 1.9°/0. The actual uncertainty in R may be more or less than one pixel depending on image quality. This error estimate applies only to random errors in edge points arising for example from digital noise in pixel intensities.

EXPERIMENTAL PROCEDURE

Before the experiment, the imaging system is aligned with respect to the HTHVESL which in turn is aligned with the gravity vector. The first step was to align the axis of the parallel levitation electrodes with respect to the gravity vector. A circular horizontal level sensor was used for this task. The second step was to rotationally align the CCD camera such that an image of either electrode produces an edge which is aligned with a row of pixels. A computer generated horizontal line which was overlaid with the flat electrode image was used to aid this process. These procedures ensure that the symmetry axis of the levitated molten sample is aligned with the vertical pixels of the CCD camera as well as with the gravity vector.

A cylindrical rod of Ni (Electronic Space Products, Int'l :99.99 % purity) was obtained. The Ni rod was cut into a small cylindrical block having a slightly larger volume than the calibration sphere. The sharp edges on the Ni cylinder were smoothened with diamond abrasive until the shape assumed roughly that of a sphere. The sample was then cleaned with ethanol and dilute nitric acid (1 part acid to 3 parts water) to remove surface impurities including the oxide layer. The sample was rinsed in water and ethanol and then dried in nitrogen gas. The sample was quickly weighed and put into the sample carousel inside the levitation chamber along with the calibration sphere. A magnetic suspension turbo pump coupled with a turbo molecular pump evacuate the HTHVESL chamber to the low 10^{-7} torr in about 4 hours.

The calibration sphere (BallTech) which has a diameter specified to within ± 2.5 microns was then levitated in HTHVESL. I-he magnification of the microscope, and the brightness, contrast and focus of the image were then adjusted. Once the optimum settings were achieved, all adjustments to the imaging system were fixed until the experiment was over. Images of the levitated calibration sphere were recorded onto video tape for later processing.

After the calibration sphere was retrieved, the Ni sample was levitated. It was slowly heated by incrementally opening the iris of the arc lamp until the sample was at about 1000 C. Sample temperature was maintained at 1000 C for 30 minutes to an hour in order to accelerate outgassing and evaporation of surface impurities from the sample.

The next procedure was to calibrate the pyrometer. The sample is superheated to a certain temperature and then allowed to cool in a purely radiative manner by extinguishing the arc lamp. This type of cooling behavior is described by Eq. (3). A typical cooling curve measured for Ni is shown in Fig. 4. The collected raw temperature data is then adjusted by changing the emissivity value until the highest

value in the isothermal region, immediately following the recalescence (indicated as #4 in Fig. 4), matched the melting temperature (T_m=1 455 C) of Ni. The temperature reading in the isothermal post-recalescence region did not remain constant. This may be due in part to the changing spectral emissivity and in part due to an actual variation in surface temperature. It fell about 7 C over 1.8 seconds duration, which is 0.48% of T_m. The emissivity determined for the Ni sample at 750 nm spectral band was 0.449. This emissivity value was then used in subsequent experiments for the live temperature readings from the pyrometer.

After the calibration procedures described above have been performed it is possible to make simultaneous temperature and density measurements on the sample. First, the sample is superheated to a desired temperature, the arc lamp is extinguished, and acquisition of temperature and video data begins as described earlier (Fig. 3). The Ni samples had a high cooling rate for which only the post-capture mode provided sufficient data in the higher temperature region. A series of superheating and radiative cooling cycles were performed while the sample was levitated, as it only took 2 minutes or less for a single cycle, The highest temperature attained during a cycle was kept low in order to avoid excessive coating of the chamber windows with metal vapor; however, it could be pushed a few hundred degrees higher at the risk of losing the significant amount of sample mass. Following the measurements the sample was cooled and retrieved. After the chamber was opened the sample was weighed once again for possible loss of the mass through evaporation. Typically for each cycle of superheating and cooling, there was about 0.6% loss of mass through evaporation.

RESULTS

After the experiment, video images of the calibration sphere and the Ni sample were transferred to the hard disk of the computer using the IMAGE CAPTURE software. Several digital images of the calibration sphere were obtained. The magnification factors for the optical system were calculated using the IMAGE CALIBRATION software described in a previous section. The magnification factors obtained from several calibration sphere images were averaged and stored in a calibration file.

The experiment involved ten superheating and cooling cycles for the Ni sample. Image data was analyzed only for the eighth cycle since it attained the deepest undercooking prior to solidification. A total of 281 sequential images of the Ni sample were captured from video tape and analyzed for the eighth cycle. This number represents a subset of the total number of frames available on the video tape since

some frames could not be used because of bad temperature or time information (Sometimes, a frame was captured during the update procedure of the temperature or the time). The IMAGE ANALYSIS program was launched to automatically analyze the volume for each image collected, with the calculation taking about 20 seconds per image. The IMAGE ANALYSIS program creates a text file containing the time, the temperature and the volume information for each image. The density and the thermal expansion coefficient for the Ni sample were then obtained by using Eqs. (1) and (2). The mass of the Ni sample measured before and after the experiment which involved 10 superheating and cooling cycles were 42,5 mg and 40.2 rng, respectively. It is therefore assumed that each cycle is responsible for a mass loss of 0.23 mg due to evaporation. The mass of the Ni sample used to calculate the density was taken as the initial mass, minus the mass loss expected through the eight cycles, giving 40.66 ± 0,23 mg.

Plotted in Fig. 5 is the density of the Ni sample measured during the cooling phase. Notice the isothermal change in density following recalescence during which a mixture of solid and liquid coexist. The solidification process generally deforms the shape of the drop somewhat so that the sample is no longer perfectly axisymmetric. The accuracy of the volume measurement for the solidified sample is therefore expected to be reduced relative to measurements of the molten state of the sample. This effect is seen in Fig. 5 as an increased scatter in the data, following solidification. Our result for the liquid density of Ni at the melting point (7.87 ± 0.09 g / cm^3) is in good agreement with the handbook value of 7.9 g / cm^3. When the density data for the solid phase of Ni is linearly extrapolated to room temperature (25 C), it yields a value of 9.02 ± 0.14 g / cm^3 which is somewhat higher than the handbook value of 8.9 g / cm^3 (see Fig. 6).

Figure 7 shows the density of the molten Ni from the present work compared with earlier studies which used EML and other methods.[3,6,7] The slope of the density versus temperature curve ($\partial \rho / \partial T$) measured here is somewhat less than measured previously. A potential cause for such a discrepancy is the presence of radial temperature gradients within the sample which will occur during radiative cooling. Such gradients would cause the measured density to be lower than it should be for a given surface temperature since the interior is hotter than the surface. A conservative estimate of the temperature gradient in this system indicates a maximum temperature difference between the surface and interior of less than 10 K. In order to observe the temperature gradient effect over the density versus temperature curve, a simple experiment was devised. The experiment consisted of performing series of

superheating and radiative cooling of a levitated test sample with each initial temperatures at equilibrium but at different values. The idea was to construct a quasi-static volume expansion curve as a function of temperature by integrating the volume data taken only at initial equilibrium temperatures for each cycle. A Ni-Zr alloy (T_m=960 C : 24% Ni and 76% Zr by composition) was chosen for a test sample because of its low vapor pressure around its melting temperature. For the duration of 18 superheating and undercooking cycles with temperatures ranging from 780 C to 1390 C, it lost less than 0.02% of the whole mass. Figure 8 shows the inverse of the relative volume expansions (normalized with the volume at 780 C for convenience) of Ni-Zr alloy made by purely radiative cooling and by quasi-static cooling. The result clearly indicate that the radial temperature gradient of the sample, when cooling purely radiatively, had a negligible effect on the slope of the acquired density curve since the inverse of the relative volume expansion is directly proportional to the density.

Figure 9 shows the volumetric thermal expansion coefficient for Ni in the liquid and solid states derived from the volume and temperature measurements. Since the mass of the sample does not enter Eq. (2), rather accurate values are obtained for the thermal expansion coefficients. The density and thermal expansion coefficient for liquid and solid Ni as a function of temperature are expressed as linear functions of temperature as follows:

$$\rho_\ell = 8.848 + 0.0006730 \times T \pm 1.1\% \qquad (1130 < T < 1565\ C)$$

$$\beta_\ell = (9.419 \times 10^{-5}) - (7.165 \times 10^{-9})\ XT \pm 0.52\% \qquad (1130\ CT < 1565\ C)$$

$$\rho_s = 9.031 + 0.0005361\ X\ T \pm 1.6\ \% \qquad (1045 < T < 1455 C)$$

$$\beta_s = (6.917 \times 10^{-5}) - (4.107 \times 10^{-9})\ XT \pm 1.0\% \qquad (1045\ CT < 1455\ C)$$

where the units are in g/cm^3 for ρ, C^{-1} for β and the C for T. The volume and the cooling profile of the sample are overlaid in Fig. 10 showing the sharp discontinuity at the recalescence point. The recalescence took place in less than two frames (1/15 second), and in order to investigate this region more carefully a high speed video camera would be necessary.

ACCURACY

In determining the accuracy of the present density measurement technique, three factors were considered; first, the error due to the scattering of the measured volume of the calibration sphere about its average value, secondly, the random noise

and the systematic error of the pyrometer that relate to the density measurement error, and thirdly, the error caused by the measurement of the mass of the sample.

In order to test the precision of the volume measurement technique, a number of images of a levitated, room-temperature calibration sphere were captured from video tape and analyzed for volume. The results of this analysis showed a standard deviation of 0.42%. The scattering of the analyzed volume is shown in Fig. 11 in the form of dimensionless quantity, the volume divided by the average value. The test was repeated by capturing the images directly from the CCD camera instead of from video tape, giving a standard deviation of 0.35%. The dispersion in these measurements arises from the collective noise in the imaging system which is generated by fluctuations in lighting, non-uniformity in focusing, optical distortion, camera misalignment, and camera and frame-grabber electronics. For the case of a liquid drop, additional noise can arise if the drop shape is non axisymmetric due to surface irregularities caused by impurities or non uniform heating. Sample glowing at high temperature is another source of error in determining the edge coordinates. Even though the edge detection relies on the intensity gradient rather than the absolute intensity of the digital image, a simulated sample glowing tests indicated as much as 0.05% discrepancy of volume. The samples used in this work appeared to be free of surface impurities, while temperature gradients along the surface arising from non uniform heating are estimated to be negligible for the type and size of samples used here. The sample glow effect is also kept minimal in this work (< O. 02%) by maintaining the relatively uniform sample to the background intensity ratio by incorporating the intense background light and the fast shutter (1/1 0000 see) speed of the CCD camera. For the case of solidified samples, some shape deformation was observed which led to greater dispersion in the volume measurements.

The accurate measurement of temperature is another crucial factor when measuring the density in relation to the temperature. The maximum random noise in the pyrometer within a single frame time was approximately ±5 C except at the point of rapid recalescence. Apart from the random noise there was a systematic error caused by the temperature calibration. The uncertainty caused by the temperature calibration was approximately 7 C arising from the variation of the temperature in the isothermal post-recalescence region. The relative error in the density which arises from an error, δT, in the temperature reading can be expressed as:

$$\frac{\delta\rho}{\rho} = \frac{1}{\rho}\left(\frac{\partial\rho}{\partial T}\right)\delta T = -\beta\,\delta T. \qquad (10)$$

A nominal temperature error for molten Ni then corresponds to a density error of approximately 0.07%.

The accuracy in the measurement of the mass of the sample depends on the vapor pressure of the molten sample at the operating temperature and vacuum level required for the HTHVESL chamber (> 10-5 torr). Therefore, the largest error in the density measurement from this experiment is expected to arise from the uncertainty in mass which is estimated to be ±0.57%, the loss of mass associated with a single superheating and cooling cycle. This is a systematic error for a given sample which can be arbitrarily reduced if one can improve the method of measurement. This error is expected to be insignificant for materials with low vapor pressure and can be significantly reduced for high vapor pressure materials by conducting the experiment with one or two cycles of superheating and cooling. Since high vapor pressure materials (such as Ni) lose mass continually through evaporation during the superheating stage, accurate determination of the sample mass becomes difficult. High vapor pressure materials also cannot be superheated very far because vapor coats the chamber windows which are needed for position control, heating and pyrometry. Density measurements with the present system will be therefore most accurate for samples of low vapor pressure; however, the higher vapor pressure case can still be carried out effectively if the experiment is performed rapidly enough to limit the significant loss of mass.

The accuracy of density measurements for solidified samples also depends on the type of material being processed. Materials which solidify by a first order phase transition, such as Ni, can show surface roughening arising from interdendritic shrinkage; however, due to its maintenance of roughly the same axisymmetrical shape upon solidification, density measurement is still possible with some loss of the accuracy due to a larger scattering. With material such as silicon whose volume expanded as it solidified, the sample shape, not only lost the axisymmetricity but it underwent a rather dramatic shape distortion. In this case the present density measurement technique was useful only during the liquid phase of the sample. Glass forming materials on the other hand, solidify by a continuous hardening process and are thus expected to show less deformation. The glass forming metal alloy $Zr_{41.2}Ti_{13.8}Cu_{12.5}Ni_{10.0}Be_{22.5}$[9] (Tm = 720 C) was seen to preserve its axisymmetric shape as well as the surface smoothness during solidification. In this case, high accuracy in the density measurements was maintained all the way to room temperature.

Highest accuracy that can be achieved for the density measurement using the current system will be the case for non evaporative material in its liquid state, incorporating the live image capture mode. The accuracy in this case will be better than 0.4%.

DISCUSSION

It should be emphasized that the current system can be modified in several ways to improve accuracy. One obvious improvement for increasing the accuracy of the volume measurement is to reduce the collective noise generated by the optical system. Possible improvements include a reduction of floor vibration, the use of a more spatially uniform background light source and the use of a higher quality video recording/retrieving system. Another obvious improvement is to reduce the uncertainty in the mass of the sample by performing the experiment in a single cycle of superheating and cooling. It is expected that such improvements can reduce the error in the density measurement to less than 0.25%. An even higher level of accuracy could be achieved by increasing image resolution by replacing the current CCD camera with a film camera (35mm or high speed motion picture) or by a higher resolution CCD camera (>1000 x 1000 pixels). Film images can be digitized with a high resolution film scanner to provide at least four times the resolution of the current CCD camera.

One significant difference between the approach described here and previous studies is that all 281 data points for the volume measurement were taken from a single sample. It should also be emphasized that the series of superheating and cooling cycles that preceded the actual measurements must have helped refine the purity of the sample by evaporating or dissolving the contaminants. Sometimes, this effect was visually apparent when a proper lighting was used on the levitated melts. One could see the surface impurities dissolving away as the temperature of the sample was raised and maintained for some period of time. Low levels of impurity are unlikely to affect the density measurement significantly, but may affect other thermophysical properties such as the surface tension or viscosity. Methods for measuring such thermophysical properties in the HTHVESL are presently being developed.

So far the materials we have tried to determine the densities in the laboratory using the HTHVESL system include nickel, silicon, aluminum, titanium alloy (Ti64), nickel-zirconium alloy and $Zr_{41.2}Ti_{13.8}Cu_{12.5}Ni_{10.0}Be_{22.5}$ glass forming alloy. The results from these materials will be published in other journals. Following a further

improvement of the present system, density measurements of many other types of metal alloys and semiconductors are planned. The HTHVESL system together with the automated data acquisition and analysis process described here allows for rapid measurement of the density of a given sample. Measurements can be made over a broad temperature range with an accuracy that may surpass most previously described methods.

ACKNOWLEDGMENTS

We thank Mr. Daniel Barber for his support throughout the experiments including the sample preparations. We also like to thank Dr. Erik Spjut for his earlier construction of the pyrometer and the temperature data acquisition. We acknowledge greatly to Dr. Yong J. Kim for his assistance with experimental work and proofreading of the manuscript. This work was carried out at the Jet F'repulsion Laboratory, California Institute of Technology, under contract with the National Aeronautics and Space Administration.

REFERENCES

[1] S. Nakamuraand T. Hibiya, Int. J. Thermophys. 13, No. 6, Nov. 1992

[2] T. lida and R. 1. L. Guthrie, The Physical Properties of Liquid Metals, Oxford University Press,1988

[3] A. E. El-Mehairy and R. G. Ward, Trans. Met. Sot. AlME, 227, 1226 (1963)

[4] T. Saito and Y. Sakuma, J. Japan Inst. Metals, 3, 1140 (1967) (in Japanese) or Transactions ISIJ, 9, 118 (1969) (in English)

[5] W. K. Rhim, S. K. Chung, D. Barber, K. F. Man, G. Gutt, A. Rulison, and R. E. Spjut, Rev. Sci. Instrum. 64, 2961 (1 993)

[6] A. D. Kirchenbaum and J. A. Cahill, Trans. ASM 56,1963,281.

[7] Lucas, L.D. Doctoral thesis, Univ. Paris, 1962.

[8] D. B. Thiessen and K. F. Man, Int. J. Thermophys. 16, 245 (1 995).

[9] A. Peker and W. L. Johnson, Appl. phys. Lett. 63, 2342, 1993

FIGURES

Fig.1 Schematic diagram of HTHVESL system (Top view) equipped for the density measurement: a) HeNe position sensing laser b) Position sensing detector c) Focusing lens d) Focusing reflector e) Side positioning electrode f) Top/bottom electrode g) Sample h) Backlight diffuser i) Fiber optical backlight j) HeNe blocking filter k) Long distance microscope 1) CCD camera m) Pyrometer n) Xenon heating lamp

Fig. 2a Flow charts for the IMAGE CAPTURE software used for live image capture and IMAGE OVERLAY software for the post image capture
Fig. 2b Flow charts for the IMAGE CALIBRATION software used for calibrating the CCD camera and the optics and IMAGE ANALYSIS software used for calculating the volume from captured image

Fig. 3 An example of output image created by overlaying the CCD image with other information such as date, time and temperature

Fig. 4 A radiative cooling curve observed for the nickel sample used in this experiment: (1 ~2) superheated stage (2-3) undercooked stage (3--4) recoalesence stage (4-5) solidification stage (5-6) further cooling after solidification

Fig. 5 Density of the nickel sample analyzed for the cooling period

Fig. 6 Density of the solid nickel at room temperature linearly extrapolated from the density of the solid nickel at high temperatures

Fig. 7 Density of the molten Ni from the present work compared with earlier studies which used EML (Ward), maximum bubble pressure (Lucas) and archimedian (Cahill & Kirshenbaum) methods.

Fig. 8 Inverse of the relative volume expansions (normalized with the volume at 780 C for convenience) made from quasi-static cooling and the purely radiative cooling are compared for Ni-Zr alloy

Fig. 9 Volumetric thermal expansion coefficient for Ni

Fig. 10 Time evolution of the volume and the temperature of the Ni are overlaid, showing the sharp reduction of the volume at the recalescence.

Fig. 11 Scattering of the volumes made from 20 calibration images measured separately. Volumes are divided by the average value.

FIG. 1

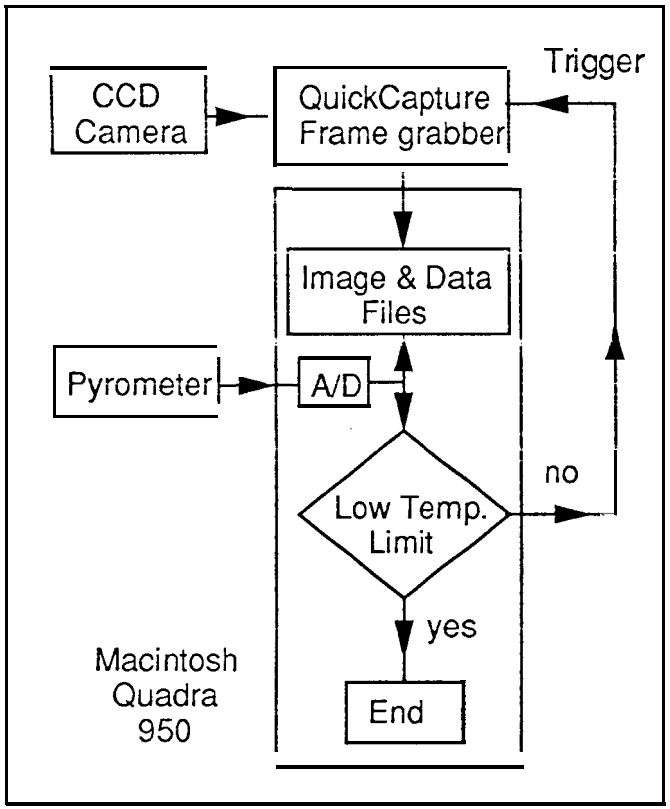

MAGE CAPTURE (LIVE)

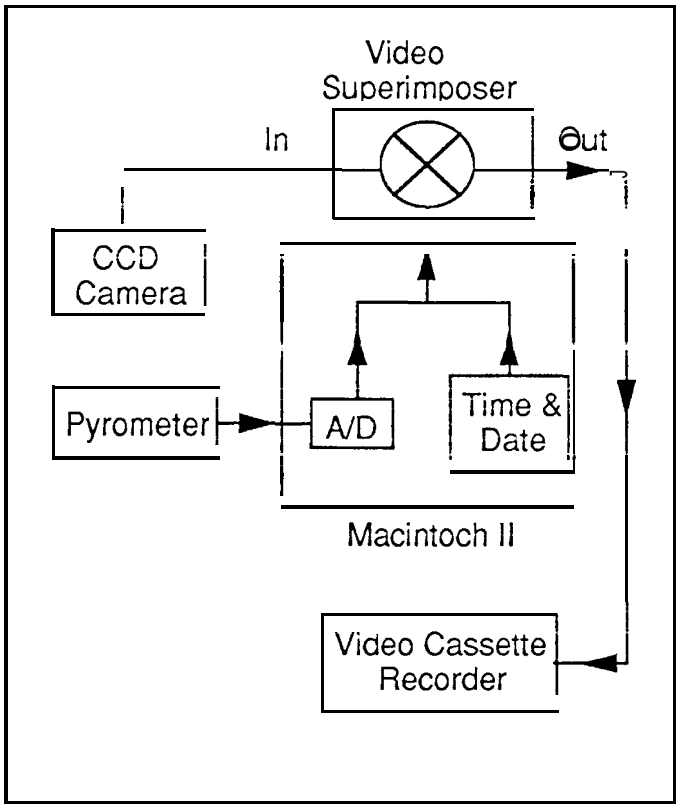

IMAGE OVERLAY (POST CAPTURE)

FIG. 2a

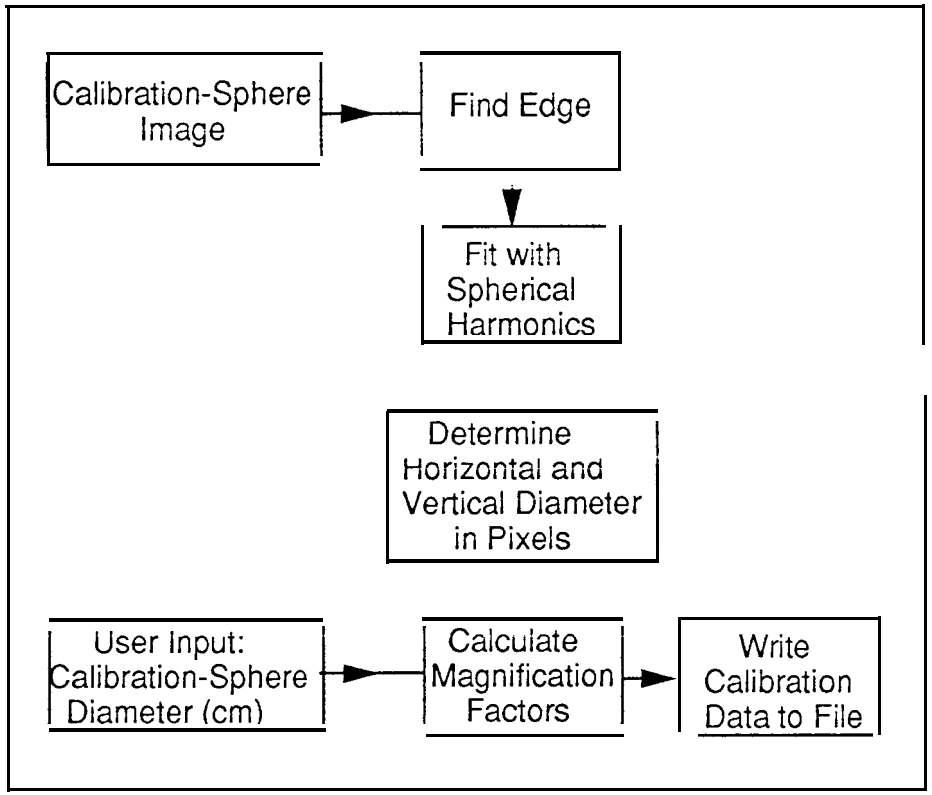

IMAGE CALIBRATION

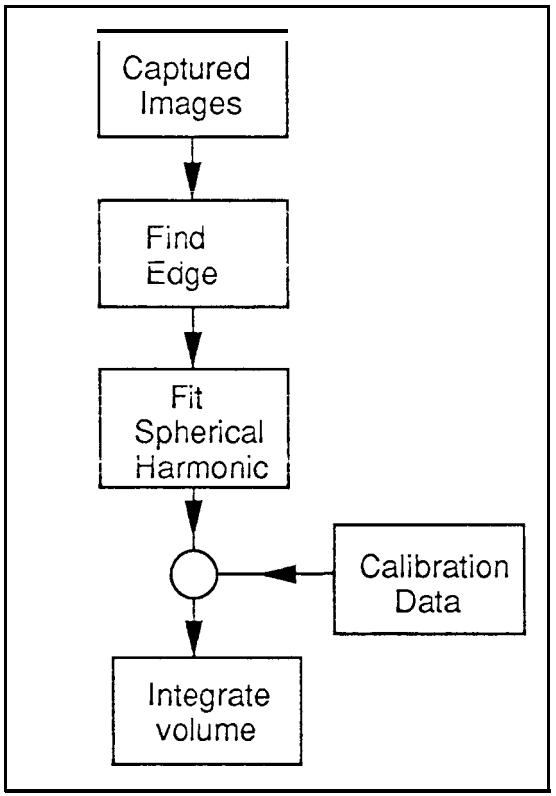

IMAGE ANALYSIS

FIG. 26

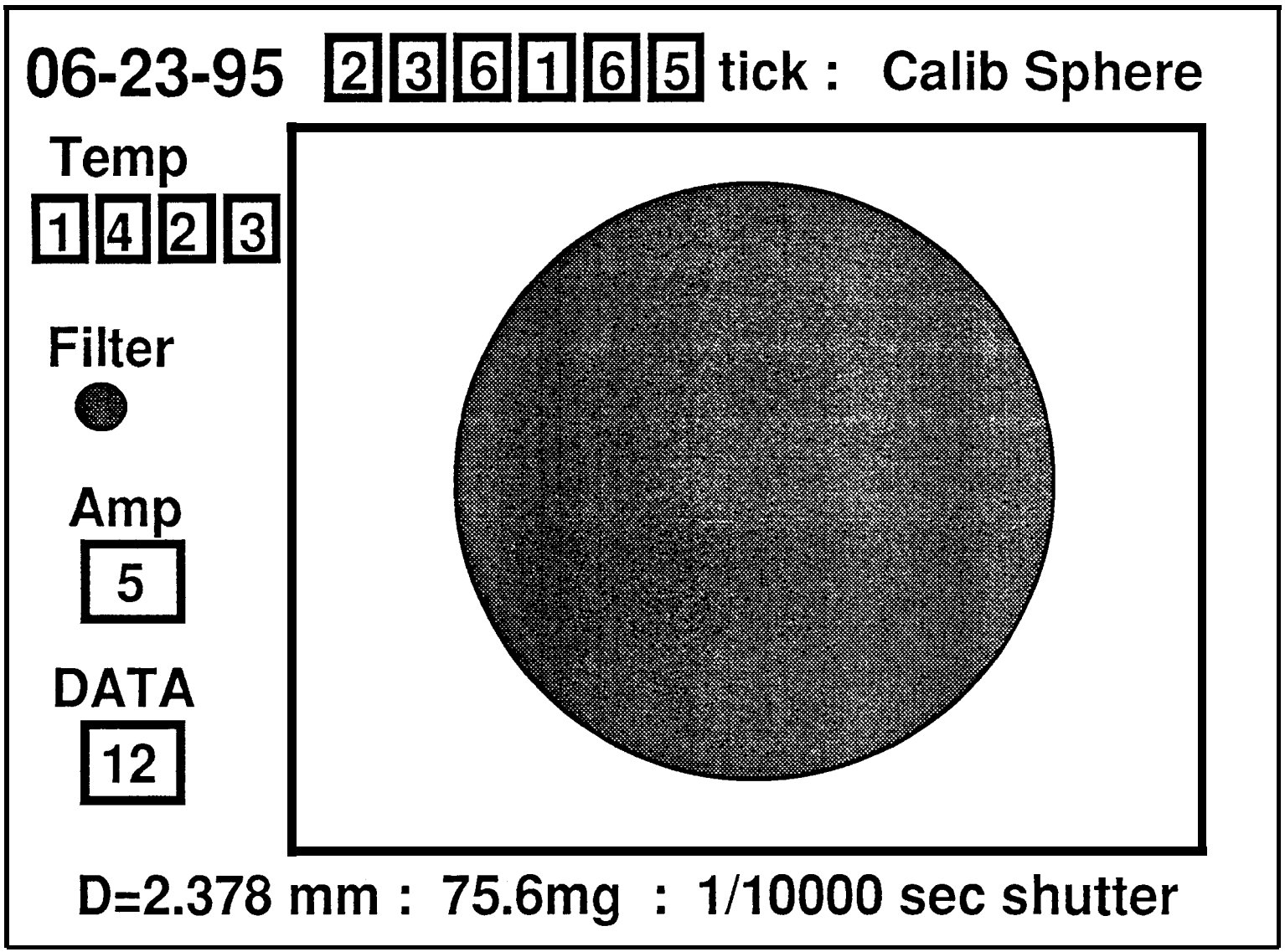
06-23-95 2 3 6 1 6 5 tick : Calib Sphere
Temp
1 4 2 3
Filter
Amp
5
DATA
12
D=2.378 mm : 75.6mg : 1/10000 sec shutter

FIG. 3

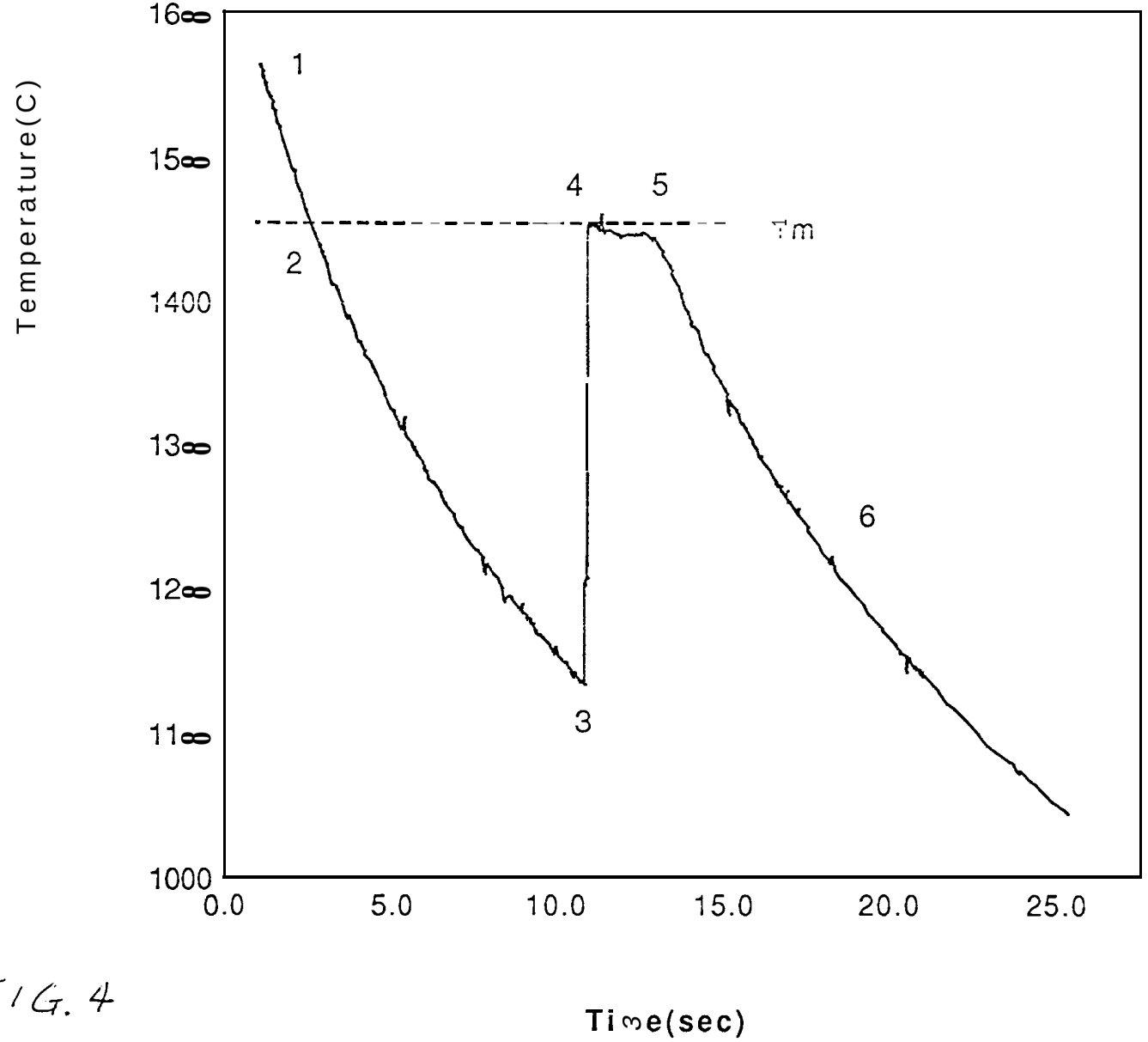
Temperature(C)
1600
1500
1400
1300
1200
1100
1000
1
2
3
4
5
6
Tm
0.0
5.0
10.0
15.0
20.0
25.0
Time(sec)

FIG. 4

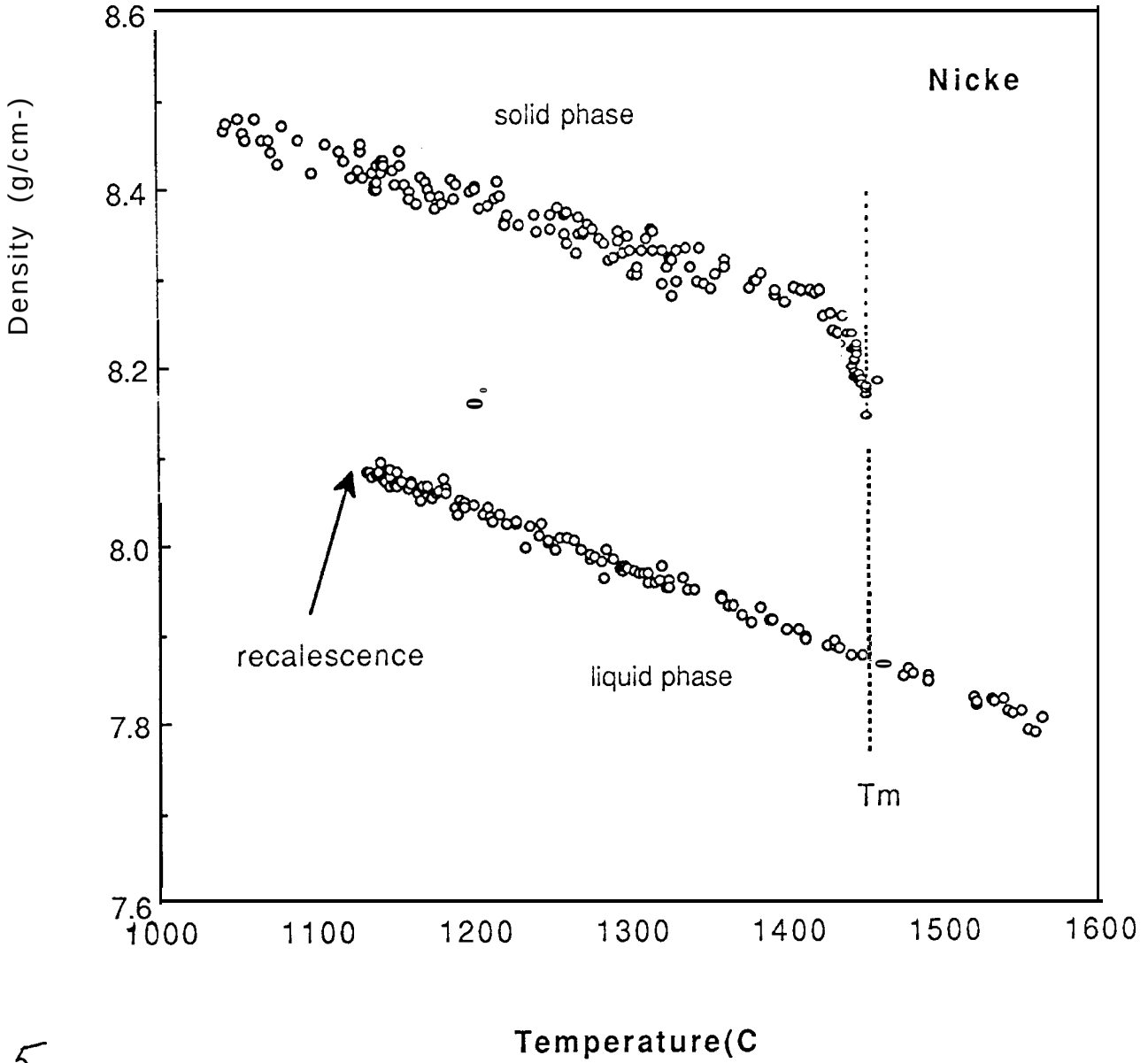
Nicke
solid phase
liquid phase
recalescence
Tm
Density (g/cm-3)
Temperature(C
8.6
8.4
8.2
8.0
7.8
7.6
1000
1100
1200
1300
1400
1500
1600

G 5

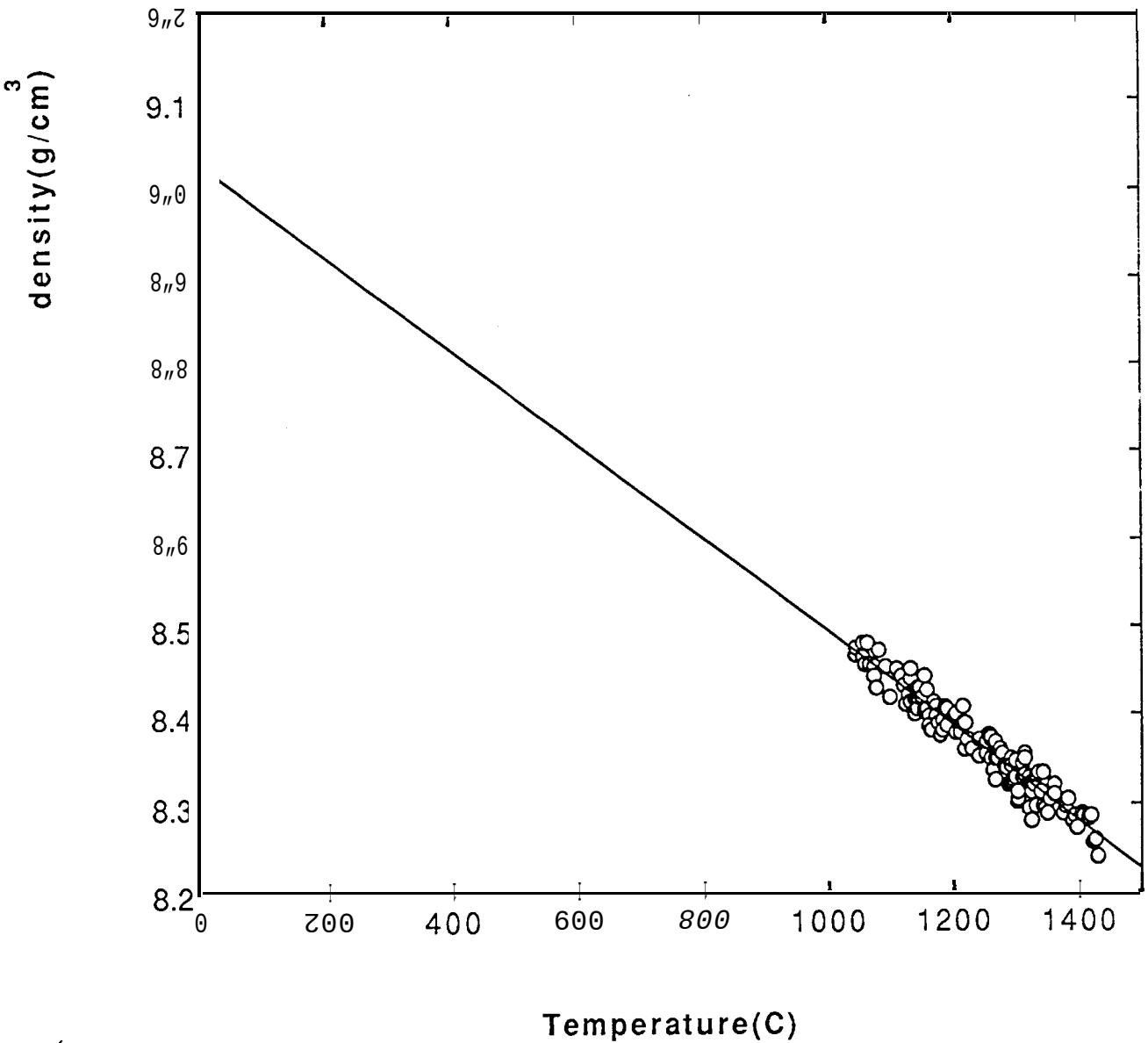
density(g/cm3)
9.2
9.1
9.0
8.9
8.8
8.7
8.6
8.5
8.4
8.3
8.2
0
200
400
600
800
1000
1200
1400
Temperature(C)

FIG. 6

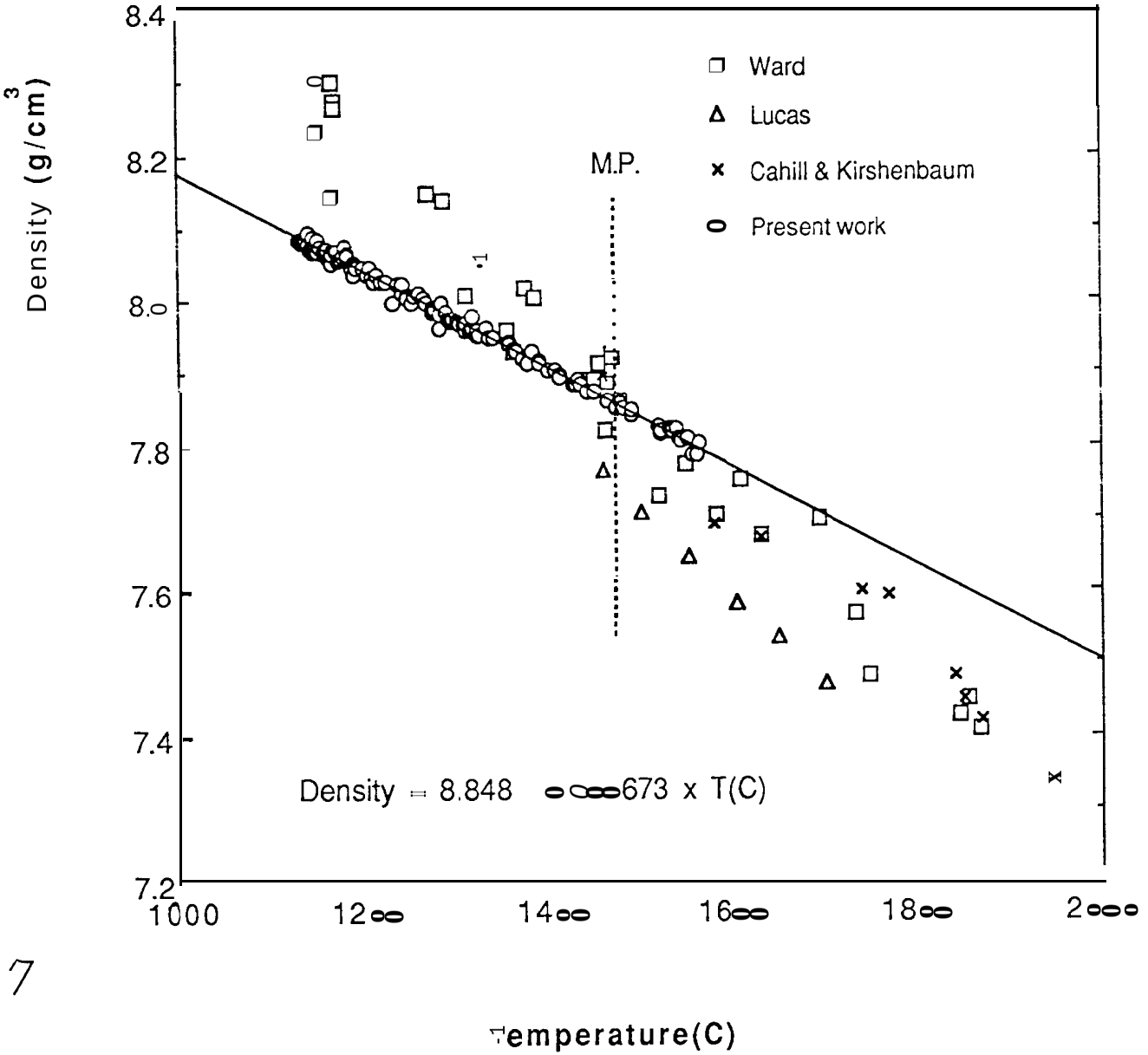
Density (g/cm^3)
8.4
8.2
8.0
7.8
7.6
7.4
7.2
1000
1200
1400
1600
1800
2000
Temperature(C)
M.P.
Ward
Lucas
Cahill & Kirshenbaum
Present work
Density = 8.848 - 673 x T(C)

FIG. 7

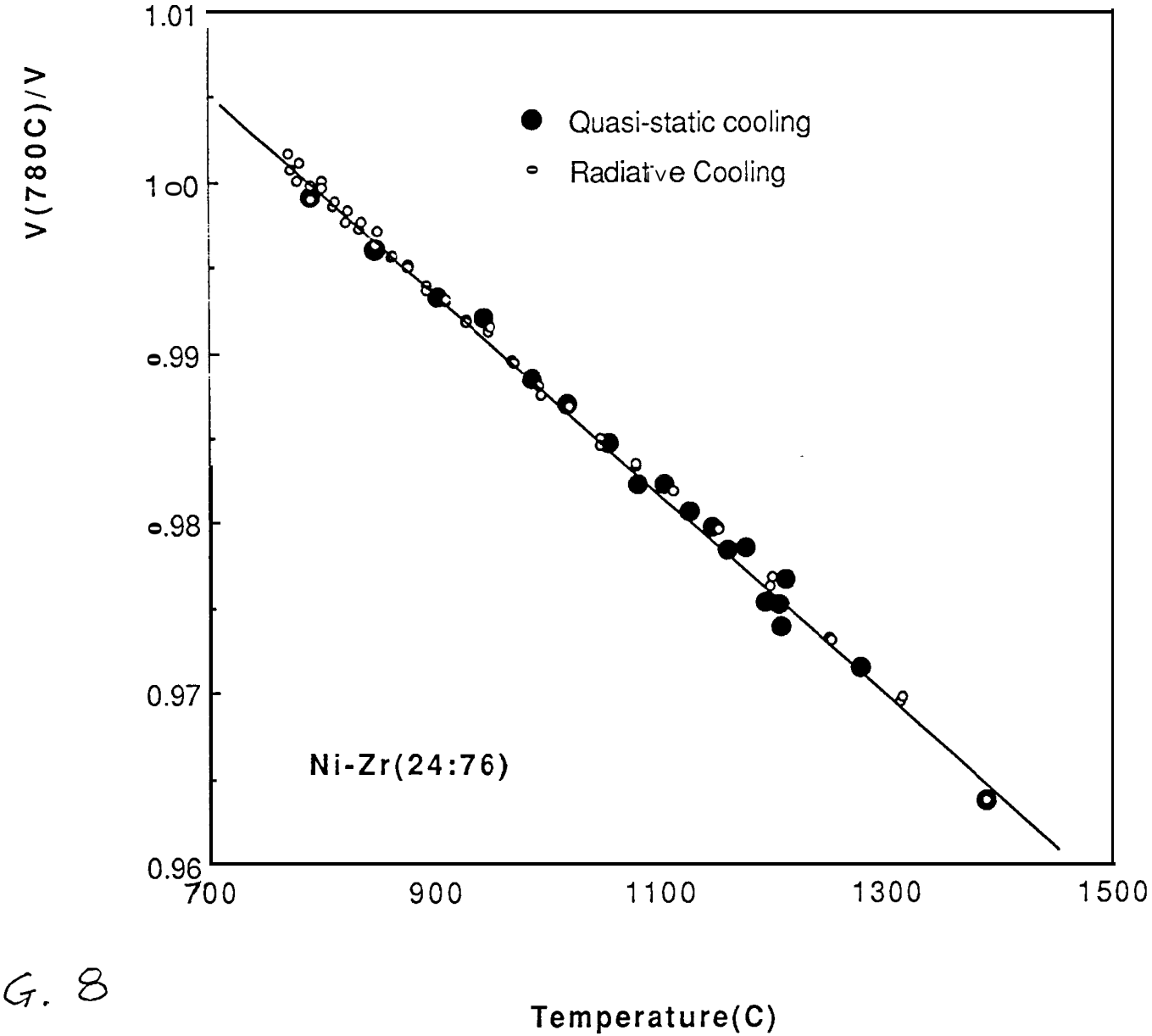
1.01
1.00
0.99
0.98
0.97
0.96
V(780C)/V
Quasi-static cooling
Radiative Cooling
Ni-Zr(24:76)
700
900
1100
1300
1500
Temperature(C)

FIG. 8

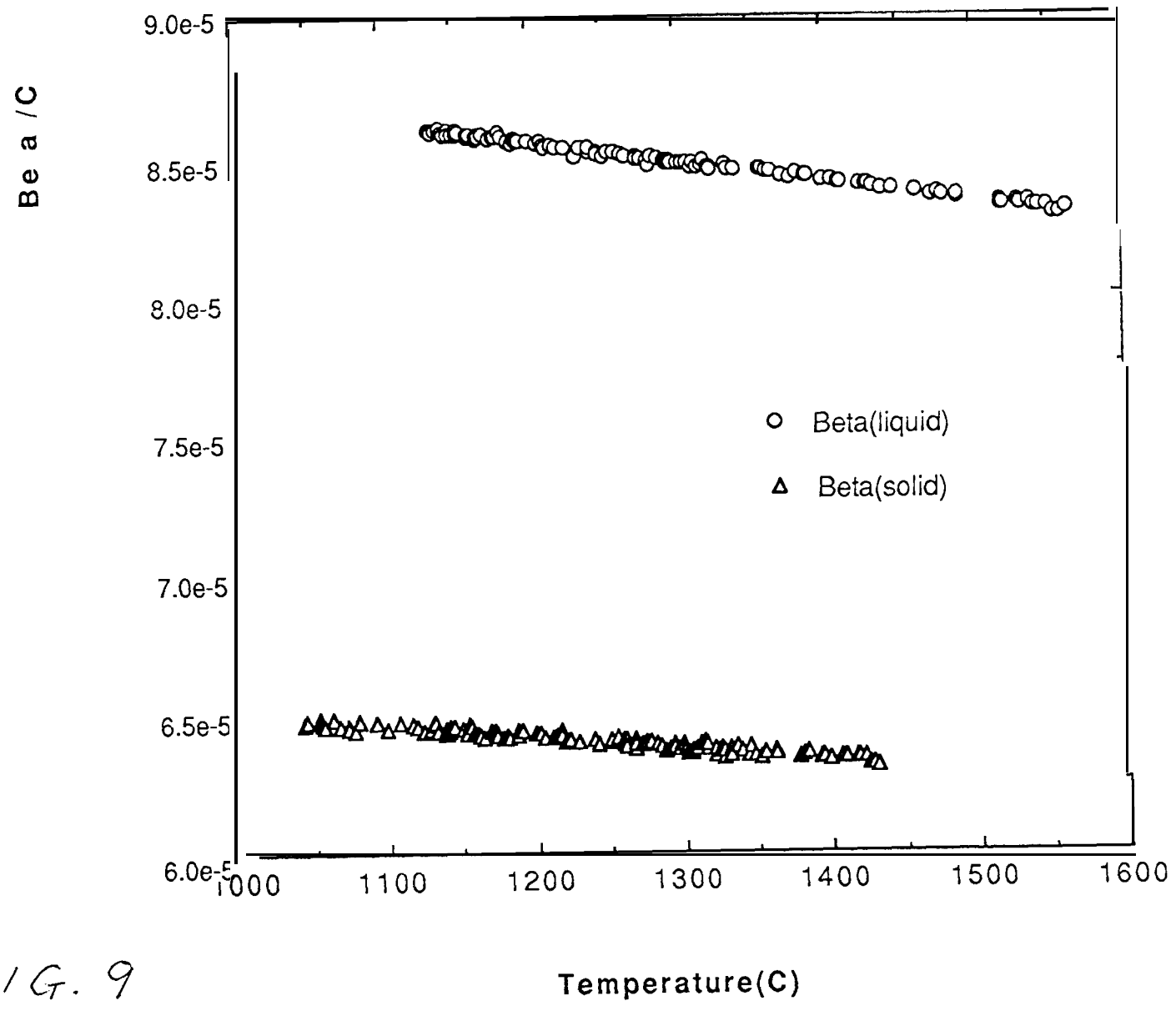
9.0e-5
8.5e-5
8.0e-5
7.5e-5
7.0e-5
6.5e-5
6.0e-5
Be a /C
Beta(liquid)
Beta(solid)
1000
1100
1200
1300
1400
1500
1600
Temperature(C)

FIG. 9

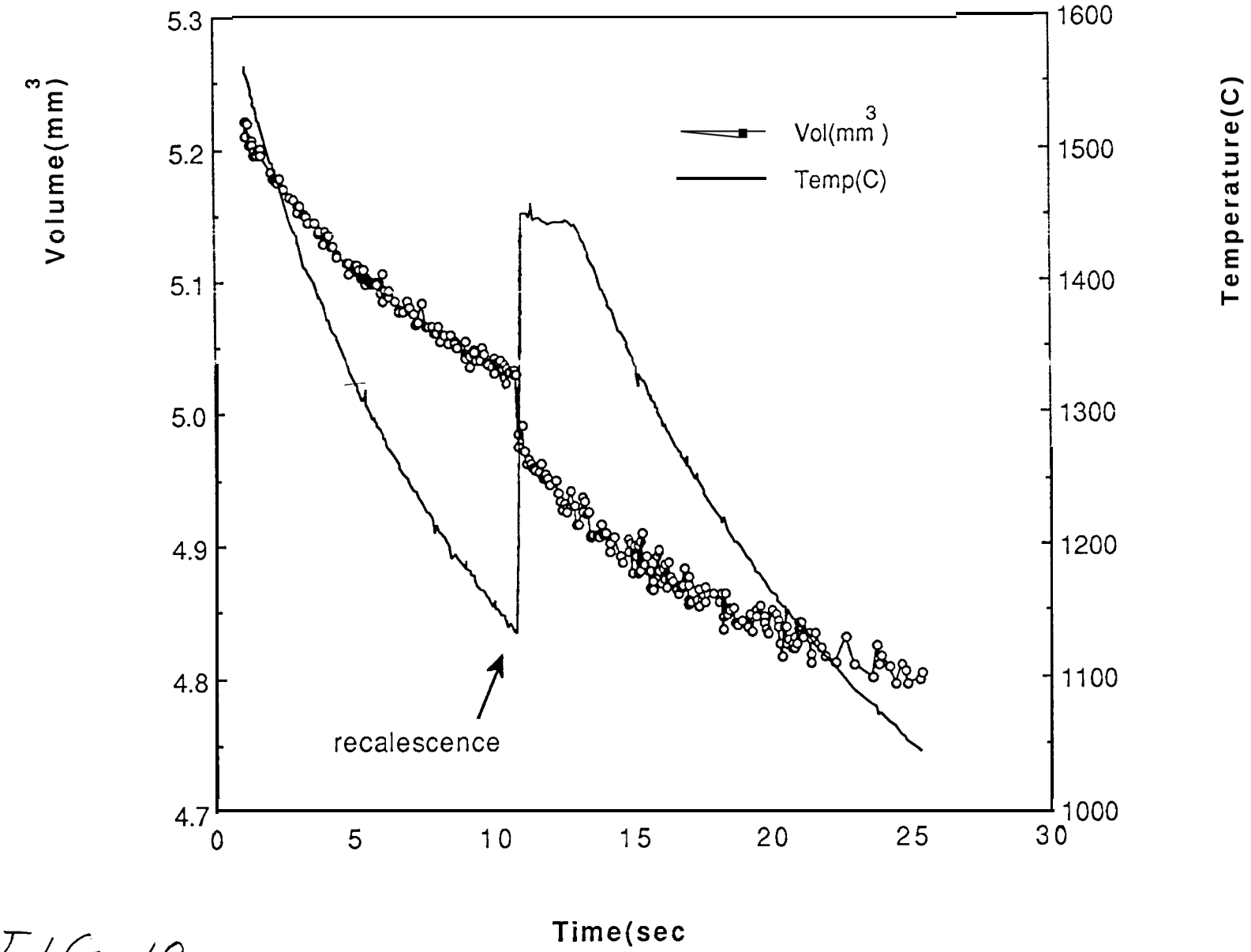
Volume(mm 3)
Temperature(C)
Time(sec
Vol(mm 3)
Temp(C)
recalescence
5.3
5.2
5.1
5.0
4.9
4.8
4.7
1600
1500
1400
1300
1200
1100
1000
0
5
10
15
20
25
30

FIG. 10

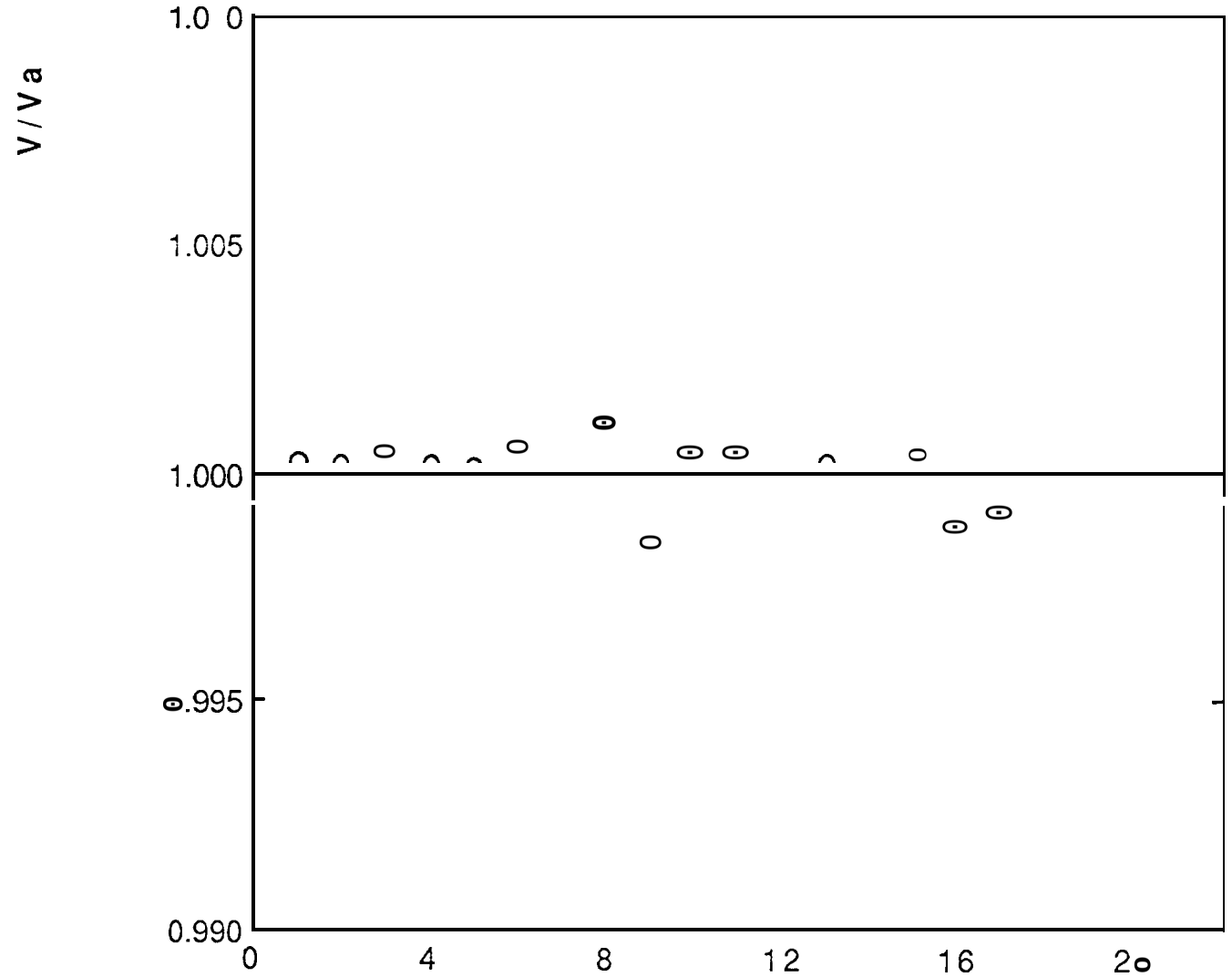

FIG. 11